energy&fuels

Article

Cite This: Energy Fuels 2019, 33, 10307−10316

pubs.acs.org/EF

Catalytic Effects on the Nonisothermal Oxidation of Solid Fuels by Oxygen: An Experimental Study

A. Nyombi,*[,†] M. R. Williams,[‡] and R. Wessling[†]

[†]Cranfield Forensic Institute and [‡]Centre for Defence Chemistry, Cranfield University—Shrivenham, Defence Academy of the United Kingdom, Shrivenham SN6 8LA, United Kingdom

Supporting Information

ABSTRACT: The role played by catalysts in solid fuel reactivity toward oxygen as a viable method for reducing toxic combustion emissions was studied. Catalyst (1 wt % Pd−Sn/alumina) treated and untreated solid fuels were analyzed using thermogravimetric analysis/differential scanning calorimetry (TGA/DSC) coupled with a gas detection system at heating rates of 20−40 °C/min and airflow rates of 30−100 mL/min. The relative CO emission factors, NO_x, CH_4, energy output, and combustion efficiency were determined as well as values of the activation energy (E_a) and pre-exponential factor (A) for the oxidation of the solid fuels. Results showed that the catalyst treatment enhanced the energy output by more than 22% and reduced CO emission factors by up to 87%. The temperature for release of nitrogen compounds was considerably reduced; however, the amounts produced were not impacted. The combustion efficiency was also improved by up to 60%. In terms of reactivity, catalyst treatment lowered the E_a for oxidation especially at $0.2 \leq \alpha \leq 0.8$. Catalyst treated samples had more free active sites on their surfaces, which decreased at temperatures of >500 °C possibly due to thermal deactivation of the catalyst. This is a viable method for minimizing toxic emissions from solid fuel combustion and enhancing energy output for domestic and industrial applications.

1. INTRODUCTION

Solid fuels (coal, lump charcoal, and charcoal briquettes) are extensively used for home and recreational cooking applications. Due to insufficient oxygen availability during combustion, fuel-rich conditions that produce toxic emission are created at mid-to-high temperatures (300−800 °C). The toxic emissions (carbon monoxide, nitrous oxide, etc.) from incomplete solid fuel combustion have caused several fatalities and chronic illnesses.[1−6]

To reduce the emissions of toxic gases from solid fuel combustion systems, technologically advanced/improved cookstoves[7−9] that use forced draft systems, with electric fans[10] and chimneys, have been used. These enhance the air circulation around the fuel improving the air-to-fuel ratio hence reducing the combustion emissions, as well as drawing out any released pollutant through the stack. Other stoves use a catalyst layer/mesh just above the solid fuel[11] to oxidize the toxic emissions during combustion while other fix the catalyst mesh in the stack of an improved cookstove[12] for the same purpose.

In domestic heaters and boilers, air-staging/two-stage combustion has been used as an effective way to reduce toxic emissions.[13] This involves supplying secondary air to aid further oxidation of flue gases from primary combustion hence reducing toxic gases.[14,15] Others use a combination of air staging and catalyst layers[16] in stacks to further oxidize unreacted toxic emissions.

The use of CO detectors/alarms[17] for warning against lethal combustion emissions has been embraced extensively. Some sensors are colorimetric,[18] forming colored complexes as the concentrations of pollutants change.[19] Others are electrochemical, which work by converting CO to CO_2 that is detected using an electrolyte[20] between a working electrode and a counter electrode. Semiconductor sensors have been the most used[21−23] employing transition metal oxides such as SnO combined with other metal oxides.

The above-mentioned methods for reducing combustion emissions work in the postcombustion mode (reducing already released emissions); hence a more robust method that minimizes toxic emissions from the source is needed. To develop a unique product that releases reduced toxic gases during cooking operations, this work draws motivation from several studies that were performed to enhance desired products during solid fuel pyrolysis/combustion/gasification. These involved the addition of catalysts on solid fuels. Inorganic mineral salts,[24] particularly potassium (K) salts,[25] decreased the temperature at which maximum degradation occurs. Char yields are also increased upon impregnation of K.[26] Potassium also reduced torrefaction time by over 28%.[27] Tungsten carbide (W_2C/alumina)[28] and molybdenum carbide (Mo_2C)/support[29] have been impregnated on biomass as effective hydrodeoxygenation agents of biomass-derived small oxygenates, phenolics, and furan derivatives. This method has been used for the selective production of aromatic hydrocarbons from lignocellulosic biomass via catalytic fast hydropyrolysis by removing sulfur, nitrogen, oxygen, and metals. In another study, waste ashes containing Al, Ca, Mg, Cu and Fe, K, Na, and Zn were impregnated with 10% Ni to enhance hydrogen-rich gas yield by over 15% from biomass.[30] Catalyst impregnation works in real time (in heterogeneous reactions)

Received: July 30, 2019
Revised: September 10, 2019
Published: September 24, 2019

DOI: 10.1021/acs.energyfuels.9b02514
Energy Fuels 2019, 33, 10307−10316

to effect desired products hence; using such a method will ensure that the cooking products (char) are safer from toxic emissions regardless of where they are used.

The objectives of this study, therefore, were to investigate and quantify the difference in reactivity of catalyst (Pd−Sn/alumina) treated charcoal briquettes (CTCB) in comparison to untreated charcoal briquettes (UTCB), commercial lump charcoal (ComC), and coal in the air (21% oxygen). Experimental studies were conducted to compare the emission of carbon monoxide, carbon dioxide, nitrogen oxides, and methane as well as the energy released from combustion and the combustion efficiency. All the experiments were carried out at different heating rates (20, 25, 30, and 40 °C/min) and airflow rates (30, 50, 80, and 100 mL/min), with temperatures ranging from 50 to 800 °C. The difference in reactivities was quantified at different conversion levels of the solid fuels in terms of activation energies and pre-exponential factors. This study expands on our previous work[31] in which catalyst impregnation was done on charcoal but the experiments were done isothermally in a tube furnace, yet real-life combustion occurs nonisothermally. Also, CO emissions were quantified and the temperature range was 300−600 °C, and finally, this study uses laboratory manufactured charcoal briquettes similar to products on the market.

2. MATERIALS AND METHODS

2.1. Materials. The CTCB and UTCB were prepared in the laboratory using in-house recipes developed to maximize the desired product. The recipes contained the following: (i) charcoal fines (<400 μm particle size) as the main fuel, wood sawdust (<400 μm particle size) as an ignition enhancer, and cassava flour as the binder for UTCB (ratio: 20:2:1); (ii) charcoal fines (<400 μm particle size) as the main fuel, wood sawdust (<400 μm particle size) as an ignition enhancer, cassava flour as the binder, and 1 wt % Pd−Sn/alumina as the catalyst for CTCB (ratio 20:2:1:0.25). The charcoal used for these recipes was prepared by laboratory pyrolysis of wood as per our previous method.[32] Appropriate amounts of water were added to the solid components and mixed thoroughly with an autoblender to form a paste that was extruded with a mold, dried, and stored for subsequent analysis. Figure 1 shows the extruded charcoal briquettes. The ComC and coal used in this study were obtained from sales stores.

2.2. Experimental Setup. The experimental setup is as shown in Figure 2. Four samples were analyzed: CTCB, UTCB, ComC, and coal. Dried powdered sample aliquots of 3−5 mg were inserted into alumina crucibles and loaded onto a Mettler Toledo TGA/DSC3+. The outlet from the chamber of the TGA/DSC was connected to a MultiRae lite gas analyzer calibrated for CO, CO_2, NO_x, and CH_4. The gas analyzer uses a pumped model operation to suck gases onto its sensors at a rate of 2 L/min. The MultiRae lite gas analyzer was programmed to autolog data at a rate of a single data point per minute. Combustion experiments were carried out nonisothermally (in triplicate) at 20, 25, 30, and 40 °C/min heating rates from 50 to 800 °C and airflow rates of 30, 50, 80, and 100 mL/min. The proximate analysis was performed as per the methods described elsewhere.[33] Since the gas analyzer pump required 2 L/min air, a connection to dry air was added to top-up the total flow during each experiment. The additional air, however, did not affect the concentration of combustion emissions analyzed since all the effluents were directed to the gas analyzer and were in such low concentrations to not overload the sensors. The gas analyzer is equipped with filters at the inlet for volatile organic compounds (VOCs), particulate matter, and moisture to avoid damage to the sensors and ensuring accuracy and reproducibility of results. Blank runs with air only were performed every after a sample run for 30 min to ensure the MultiRae lite gas analyzer was fresh for the next sample.

Figure 1. Charcoal briquettes.

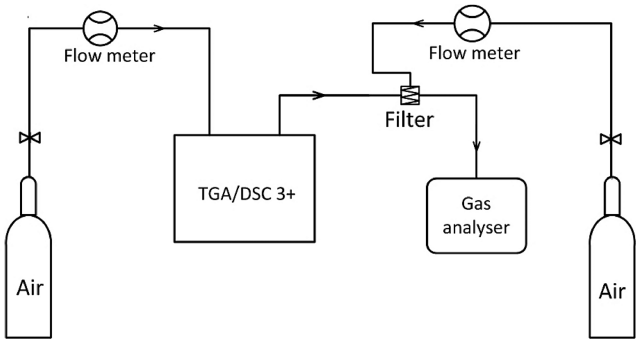

Figure 2. Experimental setup for the combined TGA/DSC and evolved gas analysis.

The computation of CO emission factors was performed as per the method described in our previous work.[34]

Specific surface areas were determined using the ASAP2020 Micromeritics surface area and porosity analyzer instrument. Samples (0.5−1.0 g) were degassed at 200 °C for 120 min. Surface area analysis was done using nitrogen and helium gases.

3. RESULTS AND DISCUSSION

3.1. General Properties of the Solid Fuels. Values for the energy released from the combustion of CTCB, UTCB, ComC, and coal as well as the proximate analysis and specific surface area are shown in Table 1. The energy produced from each solid fuel was calculated from integrals of the exotherm peaks for each run and expressed as kilojoules per gram. This energy increased with airflow due to increased oxygen availability and decreased with the heating rate. CTCB produced up to 6.7% more energy compared to UTCB, up to 22.3% more energy compared to ComC, and 14.8% more energy than commercial coal. In general, the high energy output from CTCB was attributed to enhanced combustion facilitated by oxygen adsorbed on the catalyst surfaces. The energy output of fuels analyzed was directly linked to their

DOI: 10.1021/acs.energyfuels.9b02514
Energy Fuels 2019, 33, 10307−10316

Table 1. Energy Released from Combustion, Proximate Analysis, and Specific Surface Area (SSA)[a]

	kJ/g	*M* (wt %)	FC (wt %)	VM (wt %)	*A* (wt %)	SSA (m^2/g)
CTCB	25.33 ± 0.48	1.52 ± 0.11	2.71 ± 0.20	91.8 ± 0.69	3.88 ± 0.87	67.3
UTCB	23.64 ± 1.26	1.64 ± 0.24	3.04 ± 0.50	91.0 ± 0.69	4.32 ± 0.08	78.3
ComC	19.70 ± 0.25	1.09 ± 0.24	4.8 ± 0.19	68.15 ± 1.29	25.96 ± 1.00	82.2
coal	21.57 ± 1.22	0.95 ± 0.06	3.54 ± 0.48	88.58 ± 0.33	6.93 ± 0.43	27.0

[a]CTCB, catalyst treated charcoal briquettes; UTCB, untreated charcoal briquettes; ComC, commercial charcoal; *M*, moisture content; FC, fixed carbon; VM, volatile matter; *A*, residual ash; SSA, specific surface area.

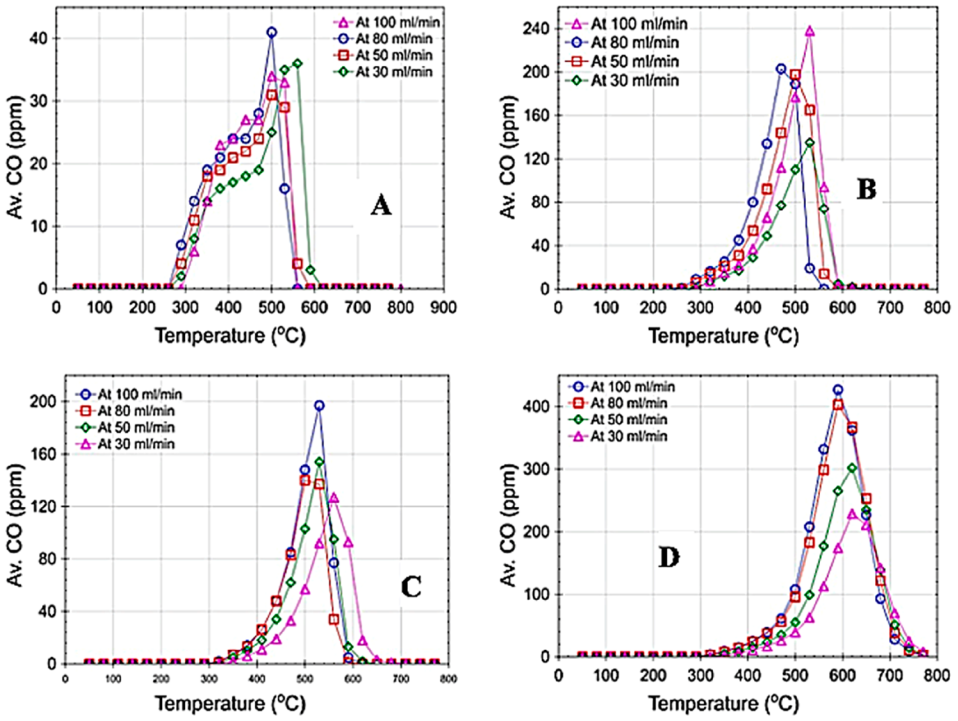

Figure 3. Average CO emissions (Av. CO) at different airflows and 30 °C/min heating rate. (A) CTCB; (B) UTCB; (C) ComC; (D) coal.

volatile matter (VM) content: the higher the VM, the higher the energy released. ComC had the highest specific surface area (SSA), while coal had the lowest SSA.

3.2. CO Emission Trends. The emission of CO from the solid fuels took different patterns during the combustion process:

(i) CTCB underwent four CO emission stages (Figure 3A). The first positive steep phase between 290 and 350 °C (CO values reaching 15 ppm as lowest and 25 ppm as highest) was attributed to release of CO from pyrolysis as a result of enhanced temperatures in sawdust and cassava binder due to the impregnated metal catalyst. Previous research has proved that metal impurities enhance the combustion temperature during combustion.[35] The second low gradient phase happened between 370 and 450 °C, in which maximum adsorption of oxygen and CO onto the catalyst surface took place resulting in maximum oxidation of CO to CO_2 (CO values increased by 2 ppm as lowest and 5 ppm as highest). The third stage happened between 470 and 500 °C, where the catalyst continuously lost activity due to sintering as temperature increased until most of the charcoal was burnt (CO values increased by 5 ppm as lowest and 15 ppm as highest). The last phase occurred between 500 and 570 °C when the remaining carbon was decomposed along with the decay of the accumulated CO.

(ii) The UTCB (Figure 3B) had an initial slow release of CO between 290 and 370 °C from pyrolysis of hemicellulose, pyrolysis of cellulose, and breakdown of unstable surface oxide complexes from sawdust and cassava binder (CO values reached about 25 ppm). The second phase was a positive steep gradient from 380 to 500 °C attributed to the decomposition of the main char matrix (CO values increased by 120 ppm as lowest and 230 ppm as highest). The last stage between 530 and 620 °C involved the breakdown of any remaining carbon as well as the washout of accumulated CO.

(iii) The ComC (Figure 3C) had an initial slow release of CO between 340 and 430 °C from the breakdown of unstable surface oxide functional groups (CO values increased to 20 ppm as lowest and 50 ppm as highest). The second positive steep stage from 440 to 500 °C corresponded to the decomposition of the main char material (CO values increased by 110 ppm as lowest and 150 ppm as highest). The last stage between 530 and 700 °C involved the breakdown of any remaining lignin in charcoal as well as the decay of accumulated CO.

(iv) Coal (Figure 3D) had an initial slow release of CO between 350 and 500 °C from the breakdown of unstable surface oxide complexes (CO values increased to 50 ppm as lowest and 110 ppm as highest). The second CO release was from 510 to 590 °C corresponding to degradation of the main carbon structure (CO values increased by 180 ppm as lowest

DOI: 10.1021/acs.energyfuels.9b02514
Energy Fuels 2019, 33, 10307−10316

and 300 ppm as highest). The last stage between 600 and 790 °C corresponded to the breakdown of the remaining stable lignin structures and decay of accumulated CO.

(v) The emission profiles took a general similar shape for all solid fuels; however, there was a general increase in peak height with an increase in airflow rate. There was also an observed shift in the peak CO emission values to higher temperatures with a decrease in airflow rates. Similarly, there was a shift of the mass loss profile to higher temperatures (Figure 2, Supporting Information) with a decrease in airflow rates. This behavior could be explained by the slow decomposition rates of samples at low airflows creating a shift in the attainment of the peak mass loss and CO emissions. Of all the solid fuels analyzed, ComC had the highest ash content. In terms of thermal stability (resistance to decomposition at high temperature), coal > ComC > UTCB ≥ CTCB.

Other plots showing the variation of mass loss and CO emissions at different heating rates and airflows are shown in Figures 1−3 of the Supporting Information.

Figure 4 shows a summary of the ratios of the CO emissions (CO emissions from one solid fuel divided by CO emissions

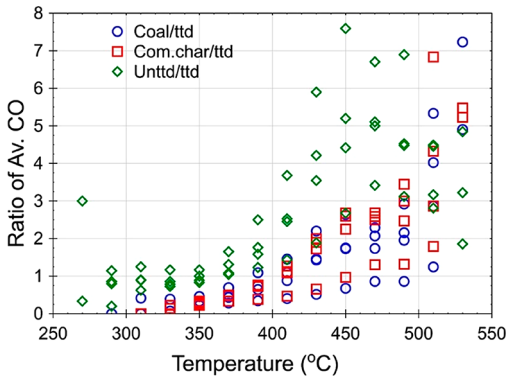

Figure 4. Ratios of average CO emissions (Av. CO) for coal/CTCB, ComC/CTCB, and UTCB/CTCB at 20 °C/min. The acronym "ttd" means treated charcoal briquettes or CTCB.

from CTCB) from the different solid fuels at 20 °C/min. We observed that UTCB emitted up to 8 times more CO than CTCB at its peak/maximum degradation stage. Even at high temperatures >500 °C when the catalyst activity had reduced, UTCB still emitted more CO than CTCB. The same analogy applies to ComC and coal. But one point to note is that, at the temperatures shown in Figure 4, coal was just in the initial phase of oxidation. Coal's maximum emissions occurred in the range from 570 to 620 °C, at which point the average CO ratio was up to 300 times compared to that of CTCB.

3.3. CO Emission Factors. Figure 5 shows the trend of CO emission factors (the average emission rate of CO relative to the initial amount of solid fuel used) calculated for different airflow rates. Three points are shown at each airflow representing different heating rates per sample. Apart from coal at 100 mL/min, all the values for each sample showed no significant differences in CO emission factors at a single airflow. However, the CO emission factors increased exponentially with an increase in airflow. Coal had the highest CO emission factors with a maximum of 155 mg/g at 100 mL/min and 20 °C/min. CTCB had the lowest CO emission factors with 2.8 mg/g at 30 mL/min and 20 °C/min. Wu et al.[36] reported that the catalyst treatment of coal tremendously reduced the combustion emissions. The UTCB and ComC

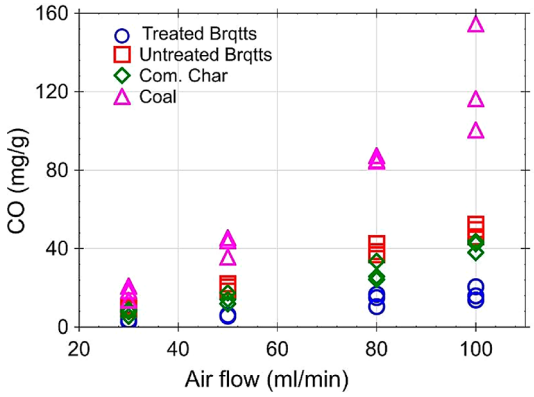

Figure 5. Overall CO emission factors as a function of airflow for Pd−Sn/alumina CTCB, UTCB, ComC, and coal.

emitted almost similar values though the former had slightly higher values (highest of 52 mg/g at 100 mL/min and lowest of 13 mg/g at 30 mL/min). From our previous work,[34] the emission factors for ComC were 257.8 mg/g at 720 mL/min, 210.9 mg/g at 1240 mL/min, 186.6 mg/g at 1710 mL/min, and 212.7 mg/g at 2200 mL/min. This trend shows that CO emission factors were generally decreasing with airflow. However, these values were obtained at isothermal temperatures ranging between 300 and 600 °C in a tube furnace and at relatively high airflows. In another study,[31] mechanically impregnated catalysts were used to minimize CO emissions from charcoal. CO emissions were reduced, but the catalyst lost activity with an increase in temperature. However, that study was also performed at isothermal temperatures yet real-life combustion takes place nonisothermally. In the present study, nonisothermal temperatures (50−800 °C) were used with different heating rates (20−40 °C/min) and low airflows (30−100 mL/min).

3.4. CO/CO_2 Ratio. The CO/CO_2 ratio is a very important property during combustion of solid fuels. High ratios are usually associated with incomplete combustion. CTCB (Figure 6A) showed a slight increase in CO/CO_2 between 300 and 370 °C, reaching the maximum ratio of ≈0.12 with a few spikes close to ≈0.23 and a continuous decline to 0.02 until all the char was burnt above 550 °C. The initial increase was due to pyrolysis reactions in sawdust and cassava flour binder as well as the breakdown of unstable carbon oxide surface complexes and other functional groups. The subsequent decline was due to increased oxidation of CO as a result of strong adsorption of oxygen and CO on catalyst surfaces resulting in enhanced reactions forming CO_2 until the final decay of accumulated combustion products from the TGA/DSC chamber. UTCB Figure 6B showed a slight increase in CO/CO_2 ratio initially to ≈0.25 at 400 °C which declined gently to 0.1 at 500 °C and then dropped sharply due to completion of char oxidation and then washing out of accumulated CO from the reaction chamber. ComC Figure 6C showed a steep rise in CO/CO_2 ratio to about 0.25 especially at 80 mL/min followed by a decline until 600 °C. Coal had a continuous increase in CO/CO_2 ratio reaching the highest recorded value in this study of slightly above 0.5 at 600 °C (Figure 6D). In general, coal had more than twice as much of the CO/CO_2 ratio compared to the other solid fuels. In our previous study,[34] the low CO/CO_2 ratio was linked to secondary reactions occurring in the pores of the charcoal promoting the conversion of CO to CO_2, whose pores are minimal in coal. This is also reflected by the

DOI: 10.1021/acs.energyfuels.9b02514
Energy Fuels 2019, 33, 10307−10316

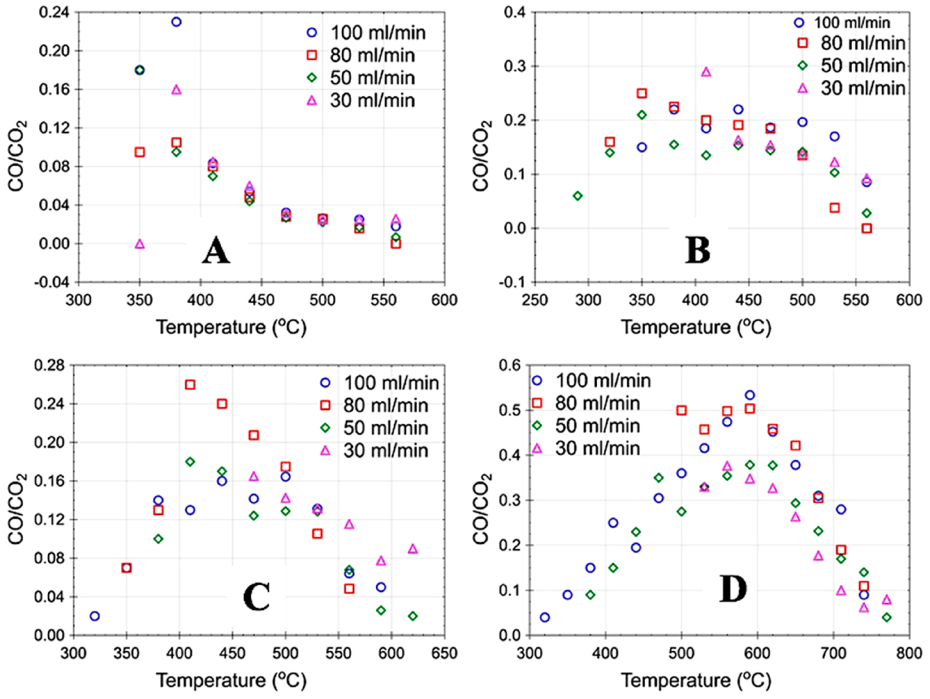

Figure 6. CO/CO_2 ratios at different airflows and 30 °C/min heating rate. (A) CTCB; (B) UTCB; (C) commercial barbecue charcoal; (D) commercial coal.

low specific surface area of coal compared to other solid fuels (Table 1). Other plots showing the variation of CO/CO_2 at different heating rates and airflow rates are given in Figures 4–6 of the Supporting Information.

The actual CO/CO_2 ratio was also predicted by manipulating experimental data using the relationship analogous to the Arrhenius equation, i.e.

$$\frac{CO}{CO_2} = A_\alpha \exp\left(-\frac{B}{T_\alpha}\right)$$

where A is a constant independent of temperature and the parameter B is analogous to an activation energy.[37,38] We developed a relationship that was used for evaluation of constants B and A at dynamic heating experiments by incorporating a heating rate, $\beta = dT/dt$. Hence, the relationship became

$$\left(\frac{CO}{CO_2}\right)\left(\frac{dt}{dT}\right) = \left(\frac{dt}{dT}\right)\left(\frac{A_\alpha}{\beta}\right)\exp\left(-\frac{B}{T_\alpha}\right)$$

Introducing natural logarithms and rearranging

$$\ln\left[\beta\left(\frac{CO}{CO_2}\right)\right]_{\alpha,k} = \ln A_{\alpha,k} - B_{\alpha,k}\left(\frac{1}{T_{\alpha,k}}\right)$$

A plot of $\ln\left[\beta\left(\frac{CO}{CO_2}\right)\right]_{\alpha,k}$ against $1000/T_{\alpha,k}$ at several kth heating rates and a particular conversion α yields straight lines in Figure 7A that were used to determine the constants B and A. In a similar study, Hu et al.[37] expressed the CO/CO_2 ratio with a universal gas constant (R = 8.314 J/mol·K) so that the constants A and B could be interpreted as relationships to pre-exponential factors and activation energy, respectively.

Tables 1 and 2 of the Supporting Information show the values obtained for the constants A and B at different conversions and airflow rates. To obtain the true values that would be used to predict the CO/CO_2 relationships for CTCB and UTCB, the natural logarithms of A (i.e., ln A) were plotted against constants B for the different airflows (Figure 7B). The point of intersection of the respective lines on the plot is the true value of ln A and constant B.

Hence, the general CO/CO_2 relationships obtained were $CO/CO_2 = 0.07\exp(0.00278/T)$ for CTCB and $CO/CO_2 = 0.2314\exp(0.00229/T)$ for UTCB. The predicted equations overestimate the CO/CO_2 though they are close to the experimental values with minimal error margins. The general trend is a decline in the ratio with an increase in temperature similar to experimental data, and the predicted UTCB values are more than 3-fold compared to CTCB. Morin et al.[38] obtained the relationship ${}^{n}CO/{}^{n}CO_2 = 6308.8\exp(-6724/T)$ for beech stick char obtained by pyrolysis at 923 K in a fluidized bed reactor. Their ratio showed an increase in CO/CO_2 ratio with temperature, the opposite of what we have obtained for CTCB. However, the ratio depends on the material being investigated,[37] among other factors.

3.5. Mass Loss Rate. As shown in Figure 8, the mass loss rate followed one main segment with a few exceptions. CTCB (Figure 8A) had the first peak at 350 °C (maximum at ≈ |3.9| %/min) attributed to the breakdown of hemicellulose, and cellulose components in sawdust and cassava binder during pyrolysis forming char. The same peak was observed with UTCB (Figure 8B), though it was relatively shorter. The decomposition of the main char and lignin components happened at 530 °C for CTCB, reaching the highest mass loss rate of |29|%/min at 80 mL/min as also observed elsewhere[36] and |27|%/min at 100 mL/min, while 30 mL/min had the lowest peak maximum mass loss rate of |24|%/min. The completion of degradation of CTCB occurred at 650 °C. UTCB reached a maximum mass loss rate of |27|%/min at 100 mL/min, while 30 mL/min still registered the lowest peak maximum of 23.5%/min. ComC peak breakdown occurred at

DOI: 10.1021/acs.energyfuels.9b02514
Energy Fuels 2019, 33, 10307−10316

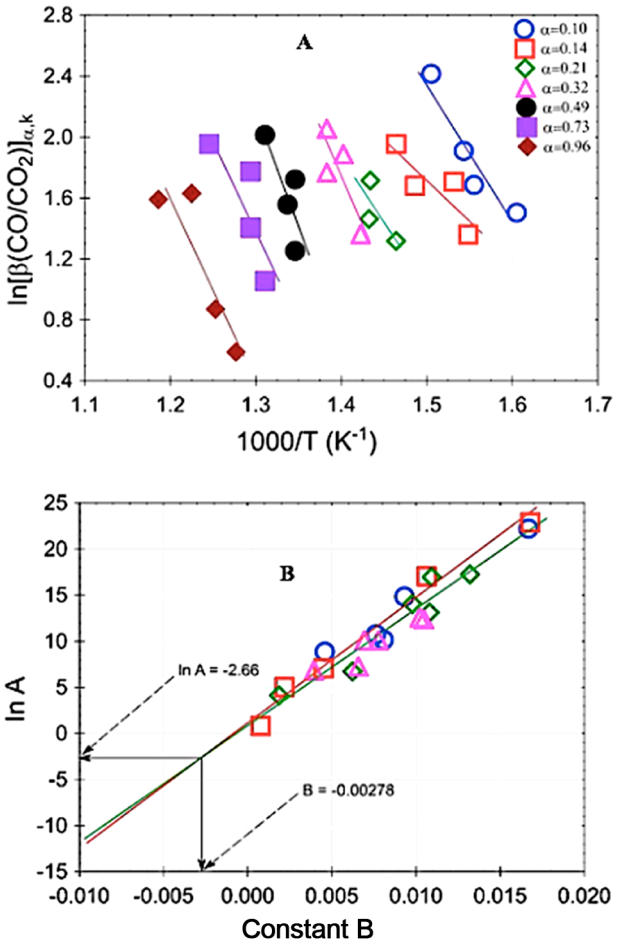

Figure 7. (A) CO/CO_2 function against $1000/T$ for determination of B and A at different conversions for UTCB. A similar plot was used for CTCB. (B) ln A against constant B for CTCB for determination of the true values of constants A and B that were used to predict the CO/CO_2 ratios.

560 °C, with |23|%/min as the maximum mass loss rate at 100 mL/min, while 50 and 30 mL/min tied on the peak maximum value of |20.7|%/min and its completion of oxidation happened at 710 °C. Coal peak decomposition happened at 620 °C, and it registered the lowest peak mass loss rate among all the samples at |18|%/min for 100 mL/min while its complete degradation occurred at 800 °C. There was a shift in the attainment of the main decomposition peak to higher temperatures with a decrease in airflow rate and an increase in heating rate. Other plots showing the variation of mass loss rate with temperature are shown in Figures 7−9 of the Supporting Information. This variation in mass loss rate was attributed to complex reactions, mass transfer, and heat transfer during the char oxidation reactions and the interaction of the char with the metal catalyst[39] in the case of CTCB.

3.6. Kinetic Parameters. Four different heating rates were used for the determination of activation energy and pre-exponential factors with the Friedman and CO−CO_2 model equations. The selection of the best fit was based on the highest regression coefficient possible. The computed values are shown in subsequent figures and tables in the Supporting Information. From now onward, more emphasis will be put on CTCB and UTCB as these have the same recipe except that CTCB has the added 1 wt % Pd−Sn/alumina catalyst. Moreover, the study was focused on comparing catalyst treatments on the oxidation behavior of solid fuels used for cooking purposes. ComC and commercial coal are also compared and discussed intermittently.

3.6.1. E_a and A Based on the Conversion Rate from Mass Loss Data. The Friedman equation[40] for determination of E_a and A was developed from $d\alpha/dt = k(T)f(\alpha)$, where $k = A\exp((-E_a)/RT)$, and takes the general form

$$\frac{d\alpha}{dt} = A_\alpha \exp\left(\frac{-E_\alpha}{RT_\alpha}\right) f(\alpha) \quad (1)$$

Introducing a heating rate $\beta = dT/dt$ and rearranging

$$\beta_k\left(\frac{d\alpha}{dT}\right)_{\alpha,k} = A_\alpha \exp\left(\frac{-E_\alpha}{RT_\alpha}\right) f(\alpha) \quad (2)$$

Introducing natural logarithms

$$\ln\left[\beta_k\left(\frac{d\alpha}{dT}\right)_{\alpha,k}\right] = \ln[A_\alpha f(\alpha)] - \frac{E_\alpha}{R}\left(\frac{1}{T_\alpha}\right) \quad (3)$$

where $f(\alpha)$ is the reaction model function at a particular kth heating rate, and α is the conversion. A plot of the left-hand side of eq 3 against $1000/T_\alpha$ should yield straight lines with gradient $-E_\alpha/R$ and intercept $\ln[A_\alpha f(\alpha)]$ (Figure 9A).

Figure 9B shows the variation of the energies of the samples at transition states with conversion for UTCB and CTCB. We observed that at low conversions $\alpha < 0.1$ (and low temperatures $T < 300$ °C), the E_a values were similar for UTCB and CTCB. This implied that the attainment of the activated complex during CTCB pyrolysis was the same as that of UTCB. At higher conversions $0.2 < \alpha < 0.8$, the E_a for CTCB continued to be lower than that for UTCB (with statistical significance) due to the catalytic action.[36] However, at high conversions $\alpha > 0.9$, the E_a values for both solid fuels were almost the same. At this conversion (and high temperatures $T > 500$ °C), the catalyst continuously lost activity due to thermal sintering and agglomeration.[41]

At low temperatures (<300 °C) and lower conversions ($\alpha < 0.1$), the major reactions involved loss of physically and chemically bound moisture and other weakly attached functional groups in endo/exothermic reactions. The addition of a catalyst enhanced the temperature and the exothermicity of the system at lower conversions (with statistical significance) and hence the positive temperature difference Figure 9C. The temperature difference dT oscillated between negative and positive (0.0 ± 5 °C) at $0.2 < \alpha < 1$ but was kept more to the negative side, meaning that catalyst treatment lowered the temperature for heterogeneous reactions during oxidation.

Assuming both the CTCB and UTCB followed a similar reaction mechanism, $f(\alpha)$, at a particular kth heating rate and α conversion, then the ratio of pre-exponential factors can be determined as follows:

$$\frac{A_{Tt,\alpha,k}}{A_{Utt,\alpha,k}} = \frac{\left(\frac{d\alpha}{dT}\right)_{Tt,\alpha,k}}{\left(\frac{d\alpha}{dT}\right)_{Utt,\alpha,k}} \exp\left[\left(\frac{E_\alpha}{RT_\alpha}\right)_{Utt,\alpha,k} - \left(\frac{E_\alpha}{RT_\alpha}\right)_{Tt,\alpha,k}\right] \quad (4)$$

where A_{Tt} and A_{Utt} are the pre-exponential factors for the CTCB and UTCB at the kth heating rate and conversion α. Using eq 4, the ratio of pre-exponential factors can be deduced

DOI: 10.1021/acs.energyfuels.9b02514
Energy Fuels 2019, 33, 10307−10316

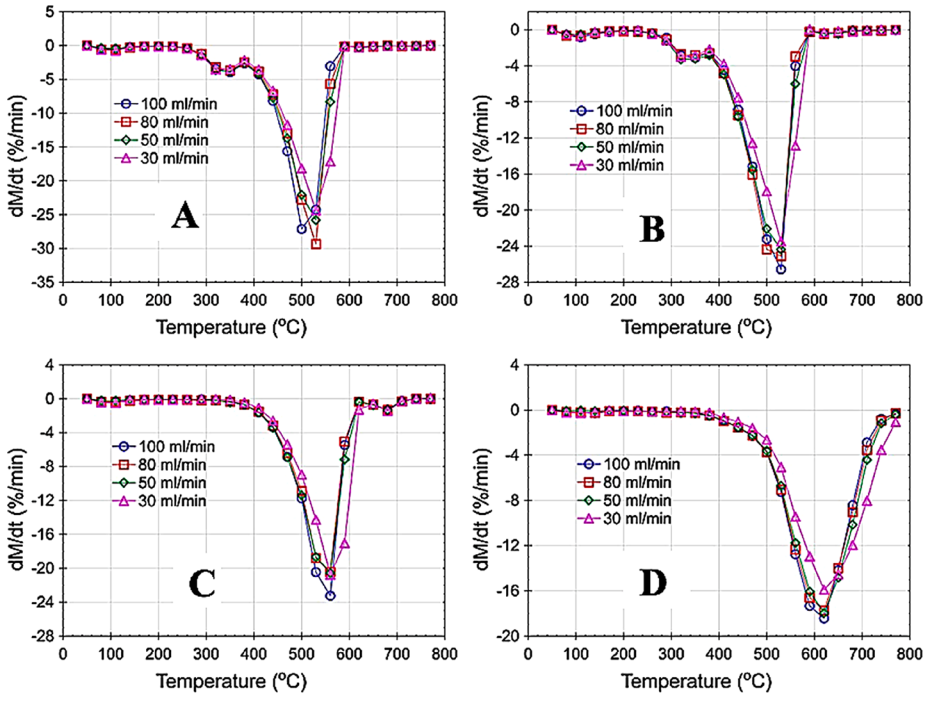

Figure 8. Mass loss rate at different airflows and 30 °C/min heating rate. (A) CTCB; (B) UTCB; (C) commercial barbecue charcoal; (D) commercial coal.

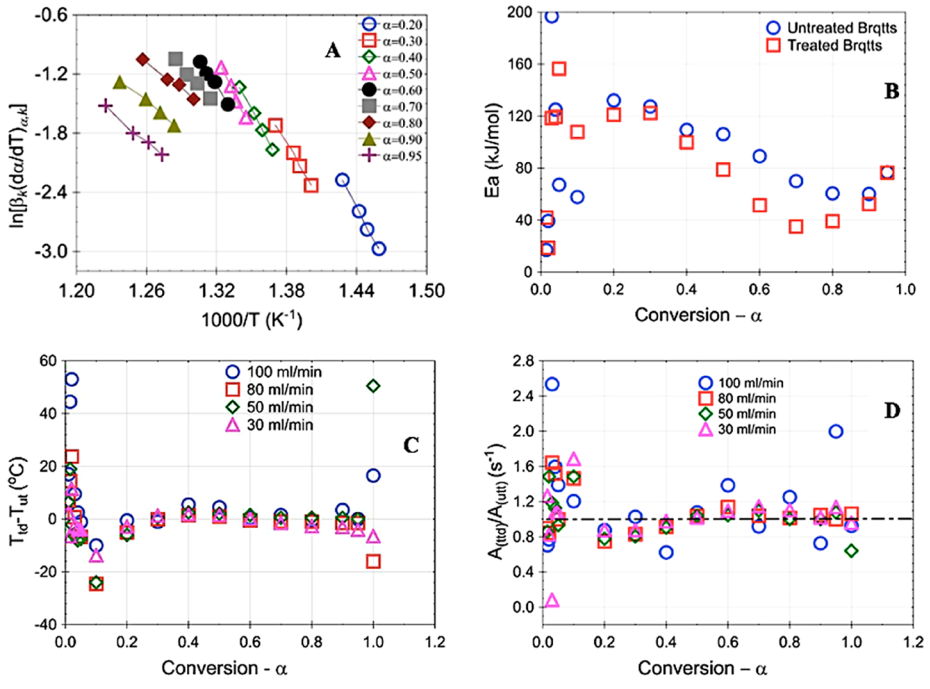

Figure 9. Plots of (A) Friedman function against 1000/T for data obtained at 100 mL/min and different heating rates for CTCB. (B) Activation energy for CTCB and UTCB at different conversions. (C) Temperature difference between CTCB and UTCB at each degree of conversion for different airflow rates. (D) Ratio of pre-exponential factors for CTCB $A_{(ttd)}$ to UTCB $A_{(utt)}$.

at different airflow rates. Equation 4 was customized for the ComC and coal.

Except for 100 mL/min airflow whose A ratios kept fluctuating up and below unity (1.0), there were general trends in A ratios for all airflows (Figure 9D). At $\alpha < 0.1$, the A ratios were mostly >1.0. Between $0.2 < \alpha < 0.5$, the A ratios were <1, while at $0.5 < \alpha < 0.9$, the A ratios were >1.0. At $\alpha > 0.9$, the A ratios were generally close to unity (1.0). In regions where A ratios were >1.0 (which are the majority—with statistical significance), the active sites on the CTCB were more compared to UTCB. This was attributed to adsorptive sites provided by the catalyst, and these sites allowed faster and quick turnover of reactions.

3.7. Methane and Combustion Efficiency. Methane is a common byproduct of solid fuel combustion. The quantity obtained depends on the C/H ratio of the solid fuel and the

DOI: 10.1021/acs.energyfuels.9b02514
Energy Fuels 2019, 33, 10307−10316

sensitivity of the analysis system. From all the samples analyzed, methane was not detected, possibly due to very low concentration.

The combustion efficiency or selectivity to CO_2 is the measure of the total emission of CO_2 as a ratio/percentage of the total carbon oxides $(CO_2/(CO + CO_2)) \times 100$. This was computed for CTCB, UTCB, ComC, and coal (Figure 10).

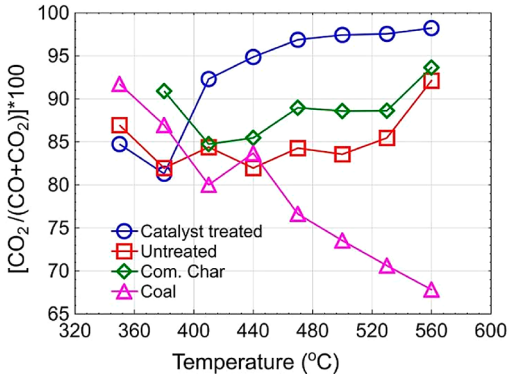

Figure 10. Plots of combustion efficiency for different solid fuels as a function of temperature.

We observed that coal had a decreasing CO_2 selectivity due to increased production of high amounts of CO as the temperature increased. The CTCB had low selectivity at temperatures <400 °C due to low oxidation of CO. At temperatures >400 °C, CTCB had rapidly increasing selectivity due to enhanced oxygen adsorption on catalyst surfaces that promoted the conversion of CO to CO_2.

3.8. Nitrogen Oxides. The combined nitrogen oxides, commonly known as NO_x, were also analyzed in this study and are presented in Figure 11. The NO_x arising from the nitrogen

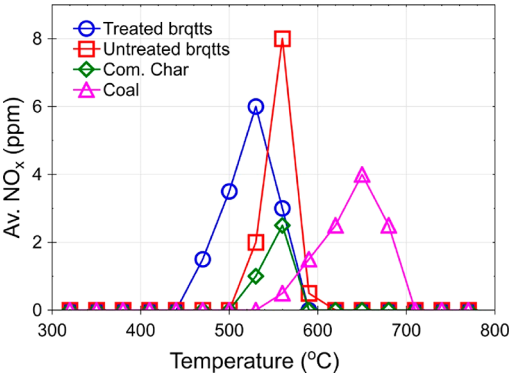

Figure 11. Scatter plots for NO_x emissions for different solid fuels.

in the fuel are termed "fuel nitrogen". Fuel nitrogen is found in plants, animal proteins, and nitrogen-rich bacteria. Reactions of amines with carboxylic groups or aldehyde groups give rise to nitrogenous species present in solid fuels which are typically bound to organic matter. Nitrogen content in solid fuels usually ranges from 0.2 to 2%.[42] Biomass fuels usually contain <1% nitrogen, while coal typically contains 1−2% nitrogen with bituminous coals usually containing 1.5−1.75% and anthracites mostly containing less than 1%.[43]

The NO_x emissions were observed starting from 440 °C for CTCB and above 500 °C for the rest of the samples. This is because nitrogen forms strong triple bonds that are not easy to break at low temperatures compared to carbon−carbon and carbon−oxygen bonds. Also, catalyst treatment reduced the temperature at which NO_x emissions were produced. We observed that, except for ComC, the areas under the curves (giving total amounts of NO_x) were not distinguishable, implying that catalyst treatment did not increase the amounts of NO_x produced. The low NO_x emissions produced by ComC could be related to its low nitrogen content as observed in our previous study.[34] However, in one study,[44] it was observed that metal impurities in biomass solid enhanced NO_x emissions during combustion.

4. CONCLUSIONS

The effect of catalyst treatment on solid fuel reactivity in an oxidative environment was studied and quantified experimentally. Two laboratory prepared biomass briquette types of catalyst (1 wt % Pd−Sn/alumina) treated charcoal briquettes (CTCB) and untreated charcoal briquettes (UTCB) were studied in addition to commercial charcoal (ComC) and coal. CO emissions and NO_x were usually affected by oxygen supply and thermal reactivity. To study how these factors affect solid fuel reactivity, nonisothermal thermogravimetric analysis in air (21% oxygen) coupled with evolved gas analysis with a robust online multisensor gas analyzer was performed. The outputs from the experiments were used to determine and compare energy outputs, CO emission factors, NO_x, combustion efficiencies, activation energies (from mass loss and CO−CO_2 emissions), and pre-exponential factors. It has been demonstrated that catalyst treatment of solid fuels enhanced their energy output by more than 22% and reduced CO emission factors by 87.1, 63.6, and 55.6% compared to coal, UTCB, and ComC, respectively. Catalyst treatment lowered the temperature at which NO_x emissions were produced but did not affect their quantity. The combustion efficiency was also improved by up to 60% compared to coal and up to 20% compared to UTCB and ComC. Treatment of solid fuels with catalyst lowered the activation energy for oxidation especially at $0.2 \leq \alpha \leq 0.8$. CTCB had more free active sites for reactions evidenced by an increased ratio of pre-exponential factors; however, the active sites decreased at temperatures >500 °C possibly due to thermal deactivation of the catalyst. Overall, this is a very promising method for minimizing toxic emissions from the combustion of solid fuels and enhancing energy output for domestic and industrial applications. However, more research is needed for thermally stable catalysts at high temperatures.

■ ASSOCIATED CONTENT

Supporting Information

The Supporting Information is available free of charge on the ACS Publications website at DOI: 10.1021/acs.energyfuels.9b02514.

Experimental TG, DTG, and relative CO emission data at different heating rates of 20, 30, and 40 °C/min; constants A and B used for predicting CO/CO_2 ratios for catalyst treated and untreated solid fuels (PDF)

■ AUTHOR INFORMATION

Corresponding Author

*E-mail: a.nyombi@cranfield.ac.uk.

ORCID

A. Nyombi: 0000-0003-0577-3099

DOI: 10.1021/acs.energyfuels.9b02514
Energy Fuels 2019, 33, 10307−10316

M. R. Williams: 0000-0001-9694-9947

Funding

This work was funded by the Gas Safety Trust (United Kingdom), Boat Safety Scheme (United Kingdom), Katie Haines Memorial Trust (United Kingdom), and Cranfield Forensic Institute (United Kingdom).

Notes

The authors declare no competing financial interest.

■ ACKNOWLEDGMENTS

The authors are thankful for the experimental support provided by Adrian Mustey and Karl Norris.

■ NOMENCLATURE

Acronyms

ComC = commercial charcoal
CTCB = catalyst treated charcoal briquettes
DSC = differential scanning calorimetry
SSA = specific surface area
TGA = thermogravimetric analysis
UTCB = untreated charcoal briquettes
VOCs = volatile organic compounds

Symbols

α = fractional conversion
β = heating rate (°C/min)
A = pre-exponential factor (s^{-1})
Al = aluminum
Ca = calcium
CH_4 = methane
CO = carbon monoxide
CO_2 = carbon dioxide
Cu = copper
E_a = activation energy (kJ/mol)
Fe = iron
K = potassium
k = rate constant (s^{-1})
Mg = magnesium
Mo_2C = molybdenum carbide
n = reaction order
Na = sodium
NO_x = nitrogen oxides
Pd = palladium
R = universal gas constant (8.314 J/mol·K)
Sn = tin
T = thermodynamic temperature (K)
t = time
V = char oxidation rate (mol/s)
W_2C = tungsten carbide
Zn = zinc

Subscript

C_0 = concentration of gaseous products at initial temperature

■ REFERENCES

(1) Chakraborty, D.; Mondal, N. K.; Datta, J. K. Indoor pollution from solid biomass fuel and rural health damage: A micro-environmental study in rural area of Burdwan, West Bengal. *Int. J. Sustainable Built Environ.* **2014**, *3* (2), 262−271.
(2) Chen, Y. Y.; Bennewith, O.; Hawton, K.; Simkin, S.; Cooper, J.; Kapur, N.; Gunnell, D. Suicide by burning barbecue charcoal in England. *J. Public Health (U. K.)* **2013**, *35* (2), 223−227.
(3) Hampson, N. B.; Kramer, C. C.; Dunford, R. G.; Norkool, D. M. Carbon Monoxide Poisoning From Indoor Burning of Charcoal Briquets. *JAMA* **1994**, *271* (1), 52−53.
(4) Winder, C. Carbon monoxide-induced death and toxicity from charcoal briquettes. *Med. J. Aust.* **2012**, *197* (6), 349−350.
(5) Nielsen, P. R.; Gheorghe, A.; Lynnerup, N. Forensic aspects of carbon monoxide poisoning by charcoal burning in Denmark, 2008−2012: An autopsy based study. *Forensic Sci., Med., Pathol.* **2014**, *10* (3), 390−394.
(6) Lyness, J. R.; Crane, J. Carbon Monoxide Poisoning From Disposable Charcoal Barbeques. *Am. J. Forensic Med. Pathol.* **2011**, *32* (3), 251.
(7) MacCarty, N.; Still, D.; Ogle, D. Fuel use and emissions performance of fifty cooking stoves in the laboratory and related benchmarks of performance. *Energy Sustainable Dev.* **2010**, *14* (3), 161−171.
(8) Njenga, M.; Iiyama, M.; Jamnadass, R.; Helander, H.; Larsson, L.; de Leeuw, J.; Neufeldt, H.; Roing de Nowina, K.; Sundberg, C. Gasifier as a cleaner cooking system in rural Kenya. *J. Cleaner Prod.* **2016**, *121*, 208−217.
(9) Njenga, M.; Mahmoud, Y.; Mendum, R.; Iiyama, M.; Jamnadass, R.; Roing de Nowina, K.; Sundberg, C. Quality of charcoal produced using micro gasification and how the new cook stove works in rural Kenya. *Environ. Res. Lett.* **2016**, *12* (9), No. 095001.
(10) Yip, F.; Christensen, B.; Sircar, K.; Naeher, L.; Bruce, N.; Pennise, D.; Lozier, M.; Pilishvili, T.; Loo Farrar, J.; Stanistreet, D.; et al. Assessment of traditional and improved stove use on household air pollution and personal exposures in rural western Kenya. *Environ. Int.* **2017**, *99*, 185−191.
(11) Obada, D. O.; Peter, M.; Kulla, D. M.; Omisanya, N. O.; Atta, A. Y.; Dodoo-Arhin, D. Catalytic abatement of CO species from incomplete combustion of solid fuels used in domestic cooking. *Heliyon* **2018**, *4* (8), e00748.
(12) Paulsen, A. D.; Kunsa, T. A.; Carpenter, A. L.; Amundsen, T. J.; Schwartz, N. R.; Harrington, J.; Reed, J.; Alcorn, B.; Gattoni, J.; Yelvington, P. E. Gaseous and particulate emissions from a chimneyless biomass cookstove equipped with a potassium catalyst. *Appl. Energy* **2019**, *235*, 369−378.
(13) Nuutinen, K.; Jokiniemi, J.; Sippula, O.; Lamberg, H.; Sutinen, J.; Horttanainen, P.; Tissari, J. Effect of air staging on fine particle, dust and gaseous emissions from masonry heaters. *Biomass Bioenergy* **2014**, *67*, 167−178.
(14) Lamberg, H.; Sippula, O.; Tissari, J.; Viren, A.; Kaivosoja, T.; Aarinen, A.; Salminen, V.; Jokiniemi, J. Operation and Emissions of a Hybrid Stove Fueled by Pellets and Log Wood. *Energy Fuels* **2017**, *31* (2), 1961−1968.
(15) Sher, F.; Pans, M. A.; Afilaka, D. T.; Sun, C.; Liu, H. Experimental investigation of woody and non-woody biomass combustion in a bubbling fluidised bed combustor focusing on gaseous emissions and temperature profiles. *Energy* **2017**, *141*, 2069−2080.
(16) Bensaid, S.; Deorsola, F. A.; Fino, D.; Russo, N. After-treatment of household wood-fired stove emissions: From catalyst formulation to full-scale system. *Catal. Today* **2012**, *197* (1), 76−89.
(17) Zhi, M.; Koneru, A.; Yang, F.; Manivannan, A.; Li, J.; Wu, N. Electrospun La0.8Sr0.2MnO3 nanofibers for a high-temperature electrochemical carbon monoxide sensor. *Nanotechnology* **2012**, *23* (30), 305501.
(18) Lin, C.; Xian, X.; Qin, X.; Wang, D.; Tsow, F.; Forzani, E.; Tao, N. High Performance Colorimetric Carbon Monoxide Sensor for Continuous Personal Exposure Monitoring. *ACS Sensors* **2018**, *3* (2), 327−333.
(19) Pannek, C.; Tarantik, K. R.; Schmitt, K.; Wöllenstein, J. Investigation of gasochromic rhodium complexes towards their reactivity to CO and integration into an optical gas sensor for fire gas detection. *Sensors* **2018**, *18* (7), 1994.
(20) Alberti, G.; Casciola, M.; Palombari, R. Amperometric sensor for carbon monoxide based on solid state protonic conduction. *Solid State Ionics* **1993**, *61* (1−3), 241−244.

DOI: 10.1021/acs.energyfuels.9b02514
Energy Fuels 2019, 33, 10307−10316

(21) Wang, C. T.; Chen, M. T. Vanadium-promoted tin oxide semiconductor carbon monoxide gas sensors. *Sens. Actuators, B* **2010**, *150* (1), 360−366.
(22) Van Geloven, P.; Honore, M.; Roggen, J.; Leppavuori, S.; Rantala, T. The influence of relative humidity on the response of tin oxide gas sensors to carbon monoxide. *Sens. Actuators, B* **1991**, *4* (1−2), 185−188.
(23) Chesler, P.; Hornoiu, C.; Mihaiu, S.; Vladut, C.; Calderon Moreno, J. M.; Anastasescu, M.; Moldovan, C.; Firtat, B.; Brasoveanu, C.; Muscalu, G.; et al. Nanostructured SnO2−ZnO composite gas sensors for selective detection of carbon monoxide. *Beilstein J. Nanotechnol.* **2016**, *7*, 2045−2056.
(24) Patwardhan, P. R.; Satrio, J. A.; Brown, R. C.; Shanks, B. H. Influence of inorganic salts on the primary pyrolysis products of cellulose. *Bioresour. Technol.* **2010**, *101* (12), 4646−4655.
(25) Lu, Q.; Zhang, Z.-X.; Wang, X.; Guo, H.-Q.; Cui, M.-S.; Yang, Y.-P. Catalytic Fast Pyrolysis of Biomass Impregnated with Potassium Phosphate in a Hydrogen Atmosphere for the Production of Phenol and Activated Carbon. *Front. Chem.* **2018**, *6*, 32.
(26) Zhou, L.; Jia, Y.; Nguyen, T.; Adesina, A. A.; Liu, Z. Hydropyrolysis characteristics and kinetics of potassium-impregnated pine wood. *Fuel Process. Technol.* **2013**, *116*, 149−157.
(27) Safar, M.; Lin, B.-J.; Chen, W.-H.; Langauer, D.; Chang, J.-S.; Raclavska, H.; Petrissans, A.; Rousset, P.; Petrissans, M. Catalytic effects of potassium on biomass pyrolysis, combustion and torrefaction. *Appl. Energy* **2019**, *235*, 346−355.
(28) Venkatesan, K.; He, S.; Seshan, K.; Selvam, P.; Vinu, R. Selective production of aromatic hydrocarbons from lignocellulosic biomass via catalytic fast-hydropyrolysis using W2C/γ-Al2O3. *Catal. Commun.* **2018**, *110*, 68−73.
(29) Machado, M. A.; He, S.; Davies, T. E.; Seshan, K.; Teixeira da Silva, V. Renewable fuel production from hydropyrolysis of residual biomass using molybdenum carbide-based catalysts: An analytical Py-GC/MS investigation. *Catal. Today* **2018**, *302*, 161−168.
(30) Al-Rahbi, A. S.; Williams, P. T. Waste ashes as catalysts for the pyrolysis−catalytic steam reforming of biomass for hydrogen-rich gas production. *J. Mater. Cycles Waste Manage.* **2019**, *21*, 1224−1231.
(31) Nyombi, A.; Williams, M. R.; Wessling, R. Mechanical impregnation of Pd-Sn/alumina and Cu-Mn/graphite on charcoal to minimise carbon monoxide emissions. *Chem. Phys. Lett.* **2019**, *715*, 181−185.
(32) Nyombi, R. W. A.; Williams, M.; Wessling. Reactivity and Free Radical Chemistry of Lilac (Syringa) Charcoal. *Energy Fuels* **2019**, *33* (2), 1227−1235.
(33) García, R.; Pizarro, C.; Lavín, A. G.; Bueno, J. L. Biomass proximate analysis using thermogravimetry. *Bioresour. Technol.* **2013**, *139*, 1−4.
(34) Nyombi, A.; Williams, M. R.; Wessling, R. Toxic emissions from smouldering combustion of woody biomass and derived char with a case study of CO build-up in an ISO container. *Energy Sources, Part A* **2019**, 1−18.
(35) Febrero, L.; Granada, E.; Regueiro, A.; Míguez, J. L. Influence of Combustion Parameters on Fouling Composition after Wood Pellet Burning in a Lab-Scale Low-Power Boiler. *Energies* **2015**, *8*, 9794−9816.
(36) Wu, Z.; Yu, Z.; Zhu, W.; Zhou, R. Energy Saving and Pollution Reducing Effects of Coal Combustion Catalysts. *Tsinghua Sci. Technol.* **2001**, *6* (2), 156−159.
(37) Hu, W.; Marek, E.; Donat, F.; Dennis, J. S.; Scott, S. A. A thermogravimetric method for the measurement of CO/CO 2 ratio at the surface of carbon during combustion. *Proc. Combust. Inst.* **2019**, *37* (3), 2987−2993.
(38) Morin, M.; Pécate, S.; Hémati, M. Kinetic study of biomass char combustion in a low temperature fluidized bed reactor. *Chem. Eng. J.* **2018**, *331*, 265−277.
(39) Larionov, K. B.; Gromov, A. A. Non-isothermal oxidation of coal with Ce(NO3)3 and Cu(NO3)2 additives. *Int. J. Coal Sci. Technol.* **2019**, *6* (1), 37−50.
(40) Rueda-Ordóñez, Y. J.; Tannous, K. Isoconversional kinetic study of the thermal decomposition of sugarcane straw for thermal conversion processes. *Bioresour. Technol.* **2015**, *196*, 136−144.
(41) Zheng, Q.; Farrauto, R.; Deeba, M. Part II: Oxidative Thermal Aging of Pd/Al2O3 and Pd/CexOy-ZrO2 in Automotive Three Way Catalysts: The Effects of Fuel Shutoff and Attempted Fuel Rich Regeneration. *Catalysts* **2015**, *5*, 1797−1814.
(42) Glarborg, P.; Miller, J. A.; Ruscic, B.; Klippenstein, S. J. Modeling nitrogen chemistry in combustion. *Prog. Energy Combust. Sci.* **2018**, *67*, 31−68.
(43) Leppälahti, J.; Koljonen, T. Nitrogen evolution from coal, peat and wood during gasification : Literature review. *Fuel Process. Technol.* **1995**, *43*, 1−45.
(44) Fournel, S.; Palacios, J. H.; Godbout, S.; Heitz, M. Effect of Additives and Fuel Blending on Emissions and Ash-Related Problems from Small-Scale Combustion of Reed Canary Grass. *Agriculture* **2015**, *5*, 561−576.

DOI: 10.1021/acs.energyfuels.9b02514
Energy Fuels 2019, 33, 10307−10316